

In silico modeling and investigation of self-heating effects in composite nano cantilever biosensors with integrated piezoresistors

Ribu Mathew and A. Ravi Sankar

Citation: *AIP Advances* **7**, 035108 (2017); doi: 10.1063/1.4977827

View online: <http://dx.doi.org/10.1063/1.4977827>

View Table of Contents: <http://aip.scitation.org/toc/adv/7/3>

Published by the [American Institute of Physics](#)

Articles you may be interested in

[Flexible bacterial cellulose / permalloy nanocomposite xerogel sheets – Size scalable magnetic actuator-cum-electrical conductor](#)

AIP Advances **7**, 035107035107 (2017); 10.1063/1.4977558

[Negative thermal expansion properties in tetragonal NbPO₅ from the first principles studies](#)

AIP Advances **7**, 035202035202 (2017); 10.1063/1.4977874

[Ab initio molecular dynamics study of temperature and pressure-dependent infrared dielectric functions of liquid methanol](#)

AIP Advances **7**, 035115035115 (2017); 10.1063/1.4978899

[Feasibility study of SWIR light absorption enhancement in PbS and PbSe nano-structure layers using surface plasmon polariton](#)

AIP Advances **7**, 035001035001 (2017); 10.1063/1.4977744

[Two-beam laser fabrication technique and the application for fabricating conductive silver nanowire on flexible substrate](#)

AIP Advances **7**, 035203035203 (2017); 10.1063/1.4978216

[An atomistic study of Y segregation at a {101⁻ 1}–{101⁻ 2} double twin in Mg](#)

AIP Advances **7**, 035308035308 (2017); 10.1063/1.4978534

HAVE YOU HEARD?

Employers hiring scientists and engineers trust

PHYSICS TODAY | JOBS

www.physicstoday.org/jobs



***In silico* modeling and investigation of self-heating effects in composite nano cantilever biosensors with integrated piezoresistors**

Ribu Mathew^a and A. Ravi Sankar^b

School of Electronics Engineering (SENSE), VIT Chennai, Chennai 600 127, India

(Received 25 October 2016; accepted 16 February 2017; published online 7 March 2017)

Over the years, piezoresistive nano cantilever sensors have been extensively investigated for various biological sensing applications. Piezoresistive cantilever sensor is a composite structure with different materials constituting its various layers. Design and modeling of such sensors become challenging since their response is governed by the interplay between their geometrical and constituent material parameters. Even though, piezoresistive nano cantilever biosensors have several advantages, they suffer from a limitation in the form of self-heating induced inaccuracy which is seldom considered in design stages. Although, a few simplified mathematical models have been reported which incorporate the self-heating effect, several assumptions made in the modeling stages result in inaccuracy in predicting sensor terminal response. In this paper, we model and investigate the effect of self-heating on the thermo-electro-mechanical response of piezoresistive cantilever sensors as a function of the relative geometries of the piezoresistor and the cantilever platform. Finite element method (FEM) based numerical computations are used to model the target-receptor interactions induced surface stress response in steady state and maximize the electrical sensitivity to thermal sensitivity ratio of the sensor. Simulation results show that the conduction mode of heat transfer is the dominant heat transfer mechanism. Furthermore, the isolation and immobilization layers play a critical role in determining the thermal sensitivity of the sensor. It is found that the shorter and wider cantilever platforms are more suitable to reduce self-heating induced inaccuracies. In addition, results depict that the piezoresistor width plays a more dominant role in determining the thermal drift induced inaccuracies compared to the piezoresistor length. It is found that for surface stress sensors at large piezoresistor width, the electrical sensitivity to thermal sensitivity ratio improves. © 2017 Author(s). All article content, except where otherwise noted, is licensed under a Creative Commons Attribution (CC BY) license (<http://creativecommons.org/licenses/by/4.0/>). [<http://dx.doi.org/10.1063/1.4977827>]

I. INTRODUCTION

In the last decade, nano-electro-mechanical systems (NEMS) based cantilever platform sensors have been utilized as investigation tools for *in-situ* explorations ranging from measurements at micro gram (μg) mass¹ to space applications.² However, in recent times much focus has been on developing piezoresistive cantilever sensors for biological sensing applications. Compared to conventional clinical diagnostic techniques like lateral flow assays (LFAs) and enzyme-linked immunosorbent assays (ELISAs), cantilever biosensors not only have the advantage of lower footprint but also have an edge due to their capability to perform real time and fast detections with lower detection limits.³ In contrast to other sensing techniques like optical,⁴ piezoelectric,⁵ capacitive,⁶ piezoresistive readout technique has several advantages in terms of label free detection, lower footprint, freedom of on or off-chip signal processing circuitry, large dynamic range, independence of operational medium,

^aE-mail: ribumathew88@gmail.com

^ba.ravishan@gmail.com

cost-effectiveness due to batch fabrication, etc. The cantilever sensor can be operated in either static or dynamic mode (where in the former relative change in cantilever deflection is measured, whereas in the later change in resonant frequency of the cantilever is gauged). Typical applications of sensing using cantilevers in dynamic mode include detection of volatile organic compound (VOC),⁷ DNA,⁸ airborne nanoparticles⁹ to cite a few. Although, dynamic mode of operation has numerous advantages, its effectiveness curtails in liquid medium due to fluid damping effect induced reduction in sensitivity and dependence of change in resonant frequency on the position of target-receptor interactions on the cantilever. In static mode of operation, cantilever end point deflection due to the target-receptor interactions induced differential stress on the opposite faces of the cantilever is measured. Typical applications of static mode operated piezoresistive nano cantilever platform biosensors include detection of cancer tissues,¹⁰ viruses,¹¹ cardiac disease markers¹² and DNA sequencing¹³ to mention a few.

Even though, piezoresistive nano cantilever sensors have numerous advantages, they suffer from a major limitation in the form of thermal drift in their output characteristics. This thermal drift in the sensor also leads to invalid detection in nano cantilever biosensors.¹⁴ Thermal drift in piezoresistive nano cantilever biosensors occur due to joule heating of the dc-excited piezoresistor. Typically, the piezoresistor is placed near the central base region of the cantilever¹⁵ which results in a non-uniform temperature profile. Joule heating induced self-heating of piezoresistive cantilever biosensors become significant due to (i) the lower thermal mass of the cantilever, and (ii) temperature dependence of the constituent material properties of the sensor. Unlike piezoresistive inertia sensors which have higher thermal mass,¹⁶ the lower thermal mass of piezoresistive cantilever sensors result in temperature induced cantilever deflection. This deflection is due to the difference in the temperature coefficient of expansion (TCE) of the constituent materials. Other parameters that contribute to the thermal drift are (i) temperature coefficient of resistance (TCR), and (ii) temperature coefficient of piezoresistance (TCP) of the doped resistor. As a result of the aforementioned factors, terminal characteristics of the sensor change even without the target-receptor interactions. Thus, the self-heating phenomenon of cantilever platform induces inaccuracy in measurement and thereby results in reliability issues. Therefore, to ensure reliable detection of target molecules by piezoresistive cantilever based sensors, it becomes imperative to understand the self-heating induced inaccuracies.

The magnitude of temperature and its spatial variation on the cantilever are a function of both the internal and external factors. The internal factors include the material and geometrical parameters of the piezoresistor and the cantilever, whereas the external factors include (i) the heat transfer mechanism i.e. conduction and convection mode, (ii) external ambient temperature, and (iii) magnitude of dc-voltage supply. Treatise encompasses a few examples where researchers have investigated the thermal drift in piezoresistive cantilever sensors through theoretical modeling¹⁷⁻¹⁹ and experimental studies.²⁰⁻²⁵ Theoretical studies have primarily focused on the impact of the piezoresistor dimensions and the external voltage supply on the thermal drift. Moreover, reported mathematical models have not only neglected the influence of cantilever dimensions and the constituent layers but also overlooked the interdependence of electrical, mechanical and thermal design parameters in determining the performance of the sensors. Similarly, the reported experimental results have mainly considered a fixed piezoresistor and cantilever sensor geometry to investigate its terminal characteristics as a function of either dc-excitation voltage and/or operational ambient. Therefore, there is a dearth of in-depth investigation which portrays the dependence of the magnitude of temperature and its spatial profile as a function of the relative dimensions of the piezoresistor and the cantilever platform.

In this paper, a systematic investigation is performed to understand the influence of relative geometries of the piezoresistor and the cantilever on the thermo-electro-mechanical response of piezoresistive cantilever biosensors. In the present study, we have considered a silicon dioxide (SiO₂) cantilever with a p-type single crystalline silicon (SCS) as the piezoresistor. The sensor is virtually fabricated with computer aided design (CAD) multi-physics numerical simulation software IntelliSuite[®] to perform coupled thermal, electrical and mechanical investigation of the sensor response. The main focus of the work includes (i) investigation of the thermal behavior of the sensor as a function of relative geometries of the piezoresistor and the cantilever, and (ii) optimization of the sensitivity

ratio $v = (\Delta R/R |_{\sigma_s}) / (\Delta R/R |_T)$, where, $\Delta R/R |_{\sigma_s}$ and $\Delta R/R |_T$ represents the relative change in the nominal resistance of the piezoresistor due to surface stress (σ_s) and temperature (T) induced effects respectively.

II. DEVICE DETAILS

The sensor considered in the present work consists of the following layers (from the bottom): (i) a structural layer, (ii) a piezoresistor, (iii) an isolation layer, and (iv) an immobilization layer. A top and a cross-sectional view of the piezoresistive nano cantilever sensor under investigation are shown in Fig. 1. When exposed to target molecules, the target-receptor binding induces change in σ_s of the cantilever surface, which results in cantilever deflection. This deflection is converted into an equivalent electrical signal by the integrated piezoresistor.

In the present study, gold (Au) is considered as the immobilization surface, since it supports a stable alkane-thiol based immobilization protocol,²⁶ typically used for the immobilization of antibodies (receptors). Translation of mechanical deflection of the cantilever into an equivalent electrical signal is a function of the structural and material parameters of the sensor. The structural parameters include the cantilever shape, lateral dimensions and thickness of the constituent layers. In the case of composite piezoresistive cantilevers, the relative distance between the mid-plane of the piezoresistor (Z_R) and neutral plane of the cantilever (Z_N) plays a critical role in governing the electrical sensitivity. To obtain maximum electrical sensitivity, the distance between the piezoresistor and neutral plane should be more. More specifics on the structural parameters and their optimization can be found in.²⁷ Material parameters which determine the electrical sensitivity include the piezoresistor gauge factor (G) and the Young's modulus (E) of the structural layer material. For a fixed cantilever geometry, electrical sensitivity depends on the ratio of the piezoresistor gauge factor (G) to the Young's modulus (E) of the structural layer i.e. G/E .²⁷ In the case of solid-state semiconductors, the combination of doped single crystalline silicon (SCS) piezoresistor and SiO_2 structural layer provides the highest G/E ratio. Therefore, in this work, we have chosen doped SCS as the piezoresistor and SiO_2 as the structural layer. To accomplish insulation of the piezoresistor from external environment, the piezoresistor is protected with a thin isolation layer. Here, SiO_2 is chosen as the isolation layer material due to its excellent electrical insulating properties and lower E .

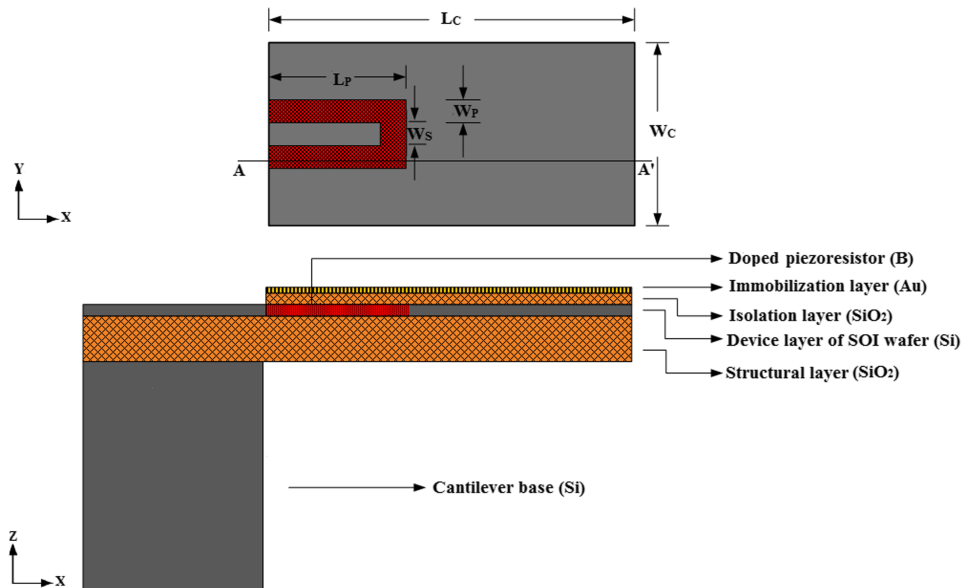


FIG. 1. A top view (without the immobilization and isolation layers) and a cross-sectional view (across AA') of the composite piezoresistive cantilever sensor with a diffused U-shaped piezoresistor. The symbols L_C and W_C represent the cantilever length and width respectively, whereas the symbols L_P , W_P , and W_S depict the piezoresistor length, width and leg space respectively. This graphic is not drawn up to the scale.

TABLE I. Dimensional details of the composite piezoresistive cantilever sensor.

Parameter	Value
Cantilever length (L_C)	200 μm
Cantilever width (W_C)	100 μm
Piezoresistor length (L_P)	60 μm
Piezoresistor width (W_P)	35 μm
Piezoresistor leg space (W_S)	30 μm
Thickness of structural SiO_2 layer	500 nm
Junction depth of the boron doped piezoresistor (t_p)	100 nm
Thickness of isolation SiO_2 layer	100 nm
Thickness of immobilization Au layer	50 nm

The device is designed in (100) silicon-on-insulator (SOI) wafers with both the cantilever and the piezoresistor length aligned along the $\langle 110 \rangle$ direction. Geometrical dimensions of the cantilever and the piezoresistor are determined by (i) the mechanical stability, and (ii) the electrical sensitivity of the sensor. Details of the parameters that influence the mechanical stability and the electrical sensitivity are explained in detail in our previous work.²⁸ Design specifications of the sensor investigated in this work include: (i) electrical sensitivity ($\Delta R/R$)/ σ_s (m/N) $> 1 \text{ E-}2$, (ii) resonant frequency (f_0) (Hz) $> 5 \text{ E}3$, (iii) spring constant (k_s) (N/m): $100 \text{ E-}3 < k_s < 10$, and (iv) measurand: surface stress (σ_s) (N/m) = $0\text{-}100 \text{ E-}3$. These specifications are typical for a piezoresistive cantilever biosensor used for antigen-antibody detection applications. The initial device dimensions (mentioned in Table I) are chosen by analytical models^{27,29} to satisfy the aforementioned specifications.

III. THEORY AND MODELING

A. Thermal model of the sensor

In piezoresistive cantilever sensors, there are mainly three modes of heat dissipation: (i) conduction, (ii) convection and (iii) radiation. The generalized thermal energy conversion equation for such a system is given by¹⁹

$$\nabla \cdot q \equiv \nabla \cdot (-k \nabla T + \rho s T u + q_r) \quad (1)$$

where, the symbols q , k , T and s represents the heat flux, thermal conductivity, temperature and heat capacity respectively. Similarly, the symbols ρ , u and q_r represents the mass density, fluid flow speed and radiation heat flux respectively. Among the three heat dissipation modes, the radiation loss from a cantilever surface is negligible, since it contributes less than 1% to the total heat dissipation even when the cantilever is heated more than 500 K.

The heat flux is generated by the dc-biased U-shaped piezoresistor integrated within the cantilever stack. The volumetric rate of heat generated in the U-shaped piezoresistor is given as

$$Q = \frac{V_b^2}{\rho_e (2L_p + W_s)^2} \quad (2)$$

where, the symbols V_b and ρ_e represents the dc-voltage and electrical resistivity of the material respectively. The 1D conduction-convection model for piezoresistive cantilever sensor is given by¹⁹

$$\lambda_{\text{eff}} A_c \frac{d^2 T}{dx^2} - hP(T - T_0) = 0 \quad (3)$$

where, λ_{eff} and x are the effective thermal conductivity of the cantilever stack and longitudinal dimension of the cantilever. The symbols A_c , P , h and T_0 represent the cross-sectional area, cantilever perimeter, heat convection coefficient and ambient temperature respectively.

The 1D temperature profile of the cantilever section with the piezoresistor is given as

$$T_{L_p}(x) = T_0 + [T_g(x) - T_0] \frac{\cosh \beta_{L_p}(L_p - x)}{\cosh \beta_{L_p} L_p}, \quad 0 < x \leq L_p \quad (4)$$

$$\text{with } \beta_{L_p} = \sqrt{\left(\frac{hP}{\lambda_{eff}}\right) A_c}$$

where, the parameter $T_g(x)$ is temperature profile of the cantilever section with piezoresistor considering only the conduction heat dissipation given as

$$T_g(x) = T_0 \cosh \sqrt{C_1} x + \frac{1}{2} C_2 x^2, \quad x \leq L_p \quad (5)$$

$$\text{where, } C_1 = \frac{\eta V_b^2 W_p t_p}{\rho_e \lambda_{eff} L_p^* V} \text{ and } C_2 = \frac{(1 - \eta T_0) V_b^2 W_p t_p}{\rho_e \lambda_{eff} L_p^* V}$$

where, L_p^* is the length of the U-shaped piezoresistor defined as $L_p^* = 2L_p + W_C - 2W_P = 2L_p + W_S$. Similarly, the symbols, η and V represent the TCR and cantilever volume with the piezoresistor. Temperature profile of the cantilever section without the piezoresistor section is given as

$$T_{L_c}(x) = T_0 + [T_{L_p}(L_p) - T_0] \frac{\cosh \beta_{L_c}(L_c - x)}{\cosh \beta_{L_c}(L_c - L_p)} \quad L_p < x \leq L_c \quad (6)$$

$$\text{where, } \beta_{L_c} = \sqrt{\left(\frac{hP}{\lambda_{eff} A_c}\right)}$$

Eq. (5) and (6) can be used to predict the temperature profile of the cantilever variation in the longitudinal direction.

B. Thermo-electro-mechanical response of the sensor

The thermo-electro-mechanical response of the composite piezoresistive cantilever sensor constitutes the relative change in nominal resistance due to target-receptor induced surface stress and thermal drift components. In the subsequent sections, we detail the sensor response to surface stress and the major components of thermal drift in the sensor output.

1. Sensor response to surface stress

For a surface stress based piezoresistive cantilever sensor with a p-type SCS piezoresistor, the electrical sensitivity is a function of the difference between longitudinal (σ_{xx}) and transverse (σ_{yy}) stress tensors given by¹⁵

$$\frac{\Delta R}{R} = \frac{\Pi_{44}}{2} (\sigma_{xx} - \sigma_{yy}) \quad (7)$$

where, Π_{44} is the magnitude of the piezoresistive coefficient of p-type SCS.

2. Thermal drift component due to TCE

Thermal drift due to difference in TCE of the constituent layers of the sensor results in bimorph deflection. For a two layered structure, the bimorph deflection is given by²⁰

$$\Delta Z_{TCE} = 3\Delta\alpha L_C^2 \Delta T \frac{(t_1 + t_2)}{t_2^2 \left(4 + 6\frac{t_1}{t_2} + 4\frac{t_1^2}{t_2^2} + \frac{E_1 t_1^3}{E_2 t_2^3} + \frac{E_2 t_2}{E_1 t_1} \right)} \quad (8)$$

where, the symbols ΔZ_{TCE} , $\Delta\alpha$, E , t_1 and t_2 represent the bimorph deflection of the cantilever, difference in TCE of the constituent layers, Young's modulus, thickness of the top layer and thickness of the bottom layer respectively. The relative change in nominal resistance due to TCE induced deflection is given by

$$\frac{\Delta R}{R} = \frac{3\Pi_1 E (Z_N - Z_R)}{2L_C^2} \Delta Z_{TCE} \quad (9)$$

where, Π_1 represents the magnitude of longitudinal piezoresistive coefficient. In the present study, for the p-type SCS piezoresistor $\Pi_1 \approx \Pi_{44/2}$.

3. Thermal drift component due to TCP

The parameter TCP (β) changes the magnitude of piezoresistive coefficient and thereby the sensor output. The relative change in the nominal resistance as a function of TCP when there is change in temperature (ΔT) is given by¹⁹

$$\frac{\Delta R}{R} = \frac{3\Pi_l(1 \pm \beta\Delta T)E(Z_N - Z_R)}{2L_C^2} \Delta Z \quad (10)$$

where, the symbol ΔZ represents the net cantilever deflection.

4. Thermal drift component due to TCR

The relative change in the nominal resistance as function of TCR (η) is given by¹⁹

$$\frac{\Delta R}{R} = \eta\Delta T \quad (11)$$

Where, ΔT is the change in temperature from the reference temperature T_0 .

5. Total response of the sensor

The sensor output is the sum of $\Delta R/R$ due to surface stress, TCE, TCP and TCR represented by eq. (12).

$$\frac{\Delta R}{R} = \eta\Delta T \pm \frac{3\Pi_l(1 \pm \beta\Delta T)E(Z_N - Z_R)}{2L_C^2} \Delta Z_{TCE} + \frac{3\Pi_l E(Z_N - Z_R)}{2L_C^2} \Delta Z_{SS} \quad (12)$$

The first term in equation represents the contribution of TCR, the second term depicts the combined effect of TCP and TCE on $\Delta R/R$, whereas the third term is the contribution of target-receptor induced surface stress.

6. Minimum detectable surface stress

The minimum detectable surface stress is a function of material and geometrical parameters of the sensor given by eq. (13)³⁰

$$\sigma_{s_{\min}} = \frac{4}{3} \sqrt{\frac{k_B T \Delta f (\rho_1)^{0.5} (E_1)^{0.5} L_C}{Q W_C}} \quad (13)$$

where, the symbols k_B , T , Δf , Q represents the Boltzmann constant, temperature, measurement bandwidth and quality factor of the sensor respectively. The material constants include ρ_1 and E_1 which are the density and Young's modulus of the structural layer respectively, whereas the geometrical parameters include cantilever length (L_C) and cantilever width (W_C).

IV. NEED FOR NUMERICAL SIMULATION

Even though, the mathematical models summarized in section III are useful in predicting the sensor response, they suffer from the following limitations: (i) the mathematical models approximate the temperature profile in 1D (only in the longitudinal direction of the cantilever), whereas the actual temperature profile is 3D which results in significant error, (ii) the mathematical models neglect the impact of sensor dimensions, especially the lateral dimensions of the cantilever, and the isolation and immobilization layers on the magnitude of temperature and its profile, and (iii) piezoresistive cantilever biosensors are multi-layered structures with different materials and constituent layer dimensions. However, the models neglect the impact of the interdependence of the material and geometrical parameters on the thermo-electro-mechanical response of the sensor. To summarize, due to the complex multi-variant design and cost intensive fabrication process of piezoresistive cantilever biosensors, it becomes vital to use a multi-physics tool to the design and modeling of such sensors.

V. SIMULATION MODEL AND SIMULATION METHODOLOGY

A. Simulation model

In this work, a finite element (FE) principle based CAD numerical simulation tool IntelliSuite[®] (version 8.7) is used to investigate the sensor characteristics. The sensor is virtually fabricated in the IntelliFAB[®] module of the software utilizing the conventional nanofabrication techniques. The sensor is designed with its base to model it closer to the actual device. A few iterative simulations were carried out to choose the base dimensions so that the cantilever base acts as a perfect heat sink with a constant temperature of 25 °C. Based on the simulations, a minimum cantilever base length, base width and base thickness of 500 μm, 100 μm, and 500 μm respectively are chosen. Adaptive mesh strategy is employed to make the computations efficient with higher number of mesh elements on the cantilever. In order to improve the computation accuracy and reduce the mesh dependence of results, mesh convergence exercises are performed. Graphic of the virtually fabricated composite piezoresistive cantilever sensor with the adaptive mesh strategy is shown in Fig 2.

The sensor responses are investigated using the Thermoelectromechanical (TEM[®]) module of the tool. The thermal, electrical and mechanical material properties imparted to the constituent layers of the sensor are listed in Table II.^{19,31,40,41} The U-shaped piezoresistor is doped with a doping concentration of $1 \text{ E}17 \text{ cm}^{-3}$ (electrical resistivity $\rho_e = 0.1966 \text{ } \Omega\text{-cm}$). Typically, the piezoresistor is excited with a dc-voltage supply ranging from 1 V to 10 V.^{12,23,27,31–34} In the present study, we have considered a dc-voltage supply of 5 V to bias the piezoresistor. In the present work, the sensor characteristics are studied by considering air as the operating medium. The external ambient temperature of the sensor is considered constant at 25 °C. Transfer of heat energy within the sensor (conduction) and its exchange with the surrounding air (convection) is modeled by imparting (i) appropriate thermal properties to the constituent layers, and (ii) convection heat transfer coefficients ($h_{\text{air}} = 200 \text{ W/m}^2 \text{ } ^\circ\text{C}$ ³⁵) to sensor surfaces. To model the sensor closer to real time operating conditions, the difference in TCE induced initial deflection of the cantilever @ zero bias voltage is incorporated in the modeling stages. More specifics of the modeling technique and details of initial deflection of the cantilever as a function of environmental temperature is reported elsewhere.³⁶ In order to mimic the target-receptor interactions, top surface of the cantilever is applied with a compressive stress of magnitude $5 \text{ E-}3 \text{ N/m}$, which is a typical in antigen-antibody interactions on Au surface.³⁷ For validating the modeling approach we have compared our computational results with the experiments reported in the literature. The thermal boundary conditions and thermal modeling approach was validated by modeling the sensor (device B) reported in Ref. 38. Temperature profile (position of the hot spot near the cantilever free end) and maximum temperature on the cantilever platform

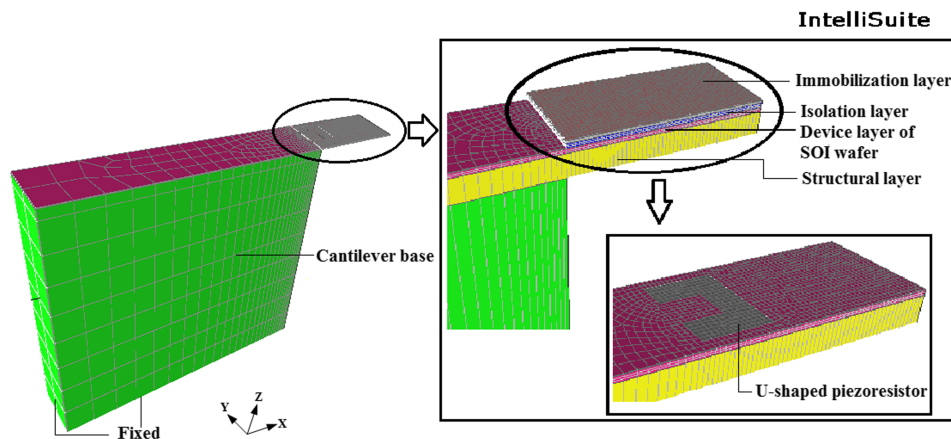


FIG. 2. A 3-D model of silicon dioxide piezoresistive cantilever sensor obtained using IntelliSuite[®] software. The graphic also contains zoom-in views of the constituent layers and the integrated U- shaped piezoresistor.

TABLE II. Material properties used in the finite element analysis.^{19,31,40}

Parameters	Boron doped Si <110>	SiO ₂	Au
Young's modulus (GPa)	169	70	80
Poisson's ratio	0.064	0.20	0.42
Density (g/cm ³)	2.32	2.22	19.30
Thermal conductivity(W/cm/°C)	1.5	1.38E-2	3.17
Thermal expansion coefficient (1E-7/°C)	28.0	5.0	142
Specific heat (J/g/°C)	712E-3	745E-3	129E-3
π_{44} (1/MPa)@1 E17cm ⁻³⁴¹	138.1E-5	-	-

(209 °C @ 10 mW input power) obtained were found to be in good agreement with the experimental results. On the other hand, the electrical and mechanical boundary conditions and their impact on the electro-mechanical response of the sensor was compared with the sensor (square cantilever-device A) reported in Ref. 39. Under surface stress loading of a few milli N/m, the sensor model (device A) depicted change in its nominal resistance (ΔR) in m Ω range that matches the experimental values.

B. Simulation methodology

This section details the methodology adopted to understand the thermal behavior and optimize the sensitivity ratio (v) of the sensor.

- (i) Initially, the U-shaped piezoresistor is operated in air, excited with a dc-voltage supply of 5V. Lateral dimensions of the piezoresistor are varied to understand the influence of the geometrical dimensions of the resistor on the magnitude of temperature and its profile.
- (ii) Similar simulations analyses are carried out by embedding the piezoresistor on the cantilever platform. In this case, the device consists of the structural layer (SiO₂) and the piezoresistor selectively doped on the device layer of SOI wafer. It may be noted that when the piezoresistor is operated in air, the dominant heat transfer mode is convection, whereas when the piezoresistor is integrated in the cantilever platform, both conduction and convection mechanisms play a significant role. In the aforementioned analyses, the cantilever dimensions are fixed at $L_C=200 \mu\text{m}$, and $W_C=100 \mu\text{m}$. Structural layer and piezoresistor thicknesses considered are 500 nm and 100 nm respectively.
- (iii) Generally, the influence of isolation and immobilization layers on the device performance is ignored by various researchers primarily to reduce the computational complexity.^{15,24,42,43} In the present work, we have included these layers and have numerically analyzed their influence on the thermo-electro-mechanical response of the sensor.
- (iv) All the above mentioned analyses were carried out at fixed cantilever dimensions. Hence, in the subsequent analyses, relative dimensions of the cantilever and the piezoresistor are varied to analyze their influence on the response of the sensor.
- (v) From the parametric analysis of the piezoresistor and the cantilever, an optimal set of cantilever lateral dimensions are chosen based on the thermal response of the sensor. Finally, dimensional optimization of the piezoresistor is performed to maximize the sensitivity ratio v . To compute the sensitivity ratio, $\Delta R/R|_{\sigma_s}$ and $\Delta R/R|_T$ of the sensor are computed separately. $\Delta R/R|_{\sigma_s}$ is computed by applying σ_s , whereas $\Delta R/R|_T$ is obtained by computing $\Delta R/R$ due to TCR, TCP and ΔZ_{TCE} individually. The TCR induced thermal drift is obtained by computing the change in the R and $\Delta R/R$, considering only the effect of TCR. TCR corresponding to T_{max} is obtained from Ref. 44. Similarly, TCP and its corresponding value of Π_{44} ⁴¹ are used to compute $\Delta R/R$. The change in $\Delta R/R$ due to ΔZ_{TCE} is obtained by imparting appropriate thermal and electrical boundary conditions without σ_s loading.

VI. RESULTS AND DISCUSSION

A. Thermal behavior of U-shaped piezoresistor operated in air and with the cantilever

1. Influence of the piezoresistor length (L_P)

The maximum steady state temperature (T_{\max}) of the U-shaped piezoresistor operated in (i) air and (ii) with the cantilever structural layer and base for different piezoresistor length is shown in Fig 3. The temperature profiles on the resistor and the cantilever platform for two different piezoresistor lengths are shown in Fig 4.

The following observations are made from Fig 3 and Fig 4.

- (i) When the piezoresistor is operated in air, T_{\max} reduces with increasing L_P . For instance, as L_P is increased from 60 μm to 180 μm , R increases by 3 times, whereas T_{\max} reduces by 4.26 times. Even though, R has a linear dependency on L_P , still the variation in T_{\max} is a non-linear function. This is due to the fact that the volumetric heat generated by the piezoresistor (Q) is a non-linear function of L_P as given by eq. (2). Therefore, when the piezoresistor is operated in air, as L_P increases, R also increases which results in a reduction in the magnitude of current in the piezoresistor, thereby resulting in lower T_{\max} . Here, the dominant mode of heat transfer is convection to the surrounding air.
- (ii) When the piezoresistor is integrated into the cantilever, the thermal behavior changes significantly. First, T_{\max} on the cantilever falls down to 39.87°C. This is 80.36% less than the T_{\max} generated when the piezoresistor of $L_P = 60 \mu\text{m}$ is operated in air. This reduction in T_{\max} is due to the dominance of heat diffusion by conduction to the cantilever base compared to heat convection to the surrounding air. Second, L_P has insignificant effect on T_{\max} . For instance, when L_P is increased from 60 μm to 180 μm , the variation in T_{\max} is less than 1%. The insignificant change in T_{\max} is due to the higher rate of heat diffusion by conduction to the cantilever base.
- (iii) From the temperature profiles it is observed that when the piezoresistor is heated in air, T_{\max} is within 2% of the average temperature on the piezoresistor. This uniform heat generation by the U-shaped piezoresistor is due to the uniform (i) doping concentration, and (ii) cross-sectional area of the piezoresistor. However, when the piezoresistor is integrated with the structural layer and the cantilever base, there is non-uniformity in the temperature profile of the cantilever. This non-uniform temperature profile on the cantilever is not only due to the non-uniform coverage of piezoresistor but also due to the contribution of two heat dissipation mechanism (i) heat diffusion to the base by conduction, and (ii) dissipation to the surrounding air by convection.

When we compare the temperature behaviour of the cantilever platform with the U-shaped piezoresistor (without isolation and immobilization layers) predicted by analytical eq. (4) and the

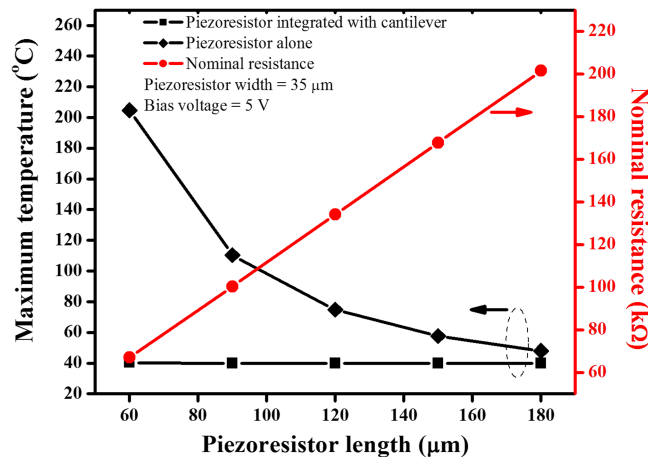


FIG. 3. Maximum cantilever temperature and nominal resistance as a function of the piezoresistor length.

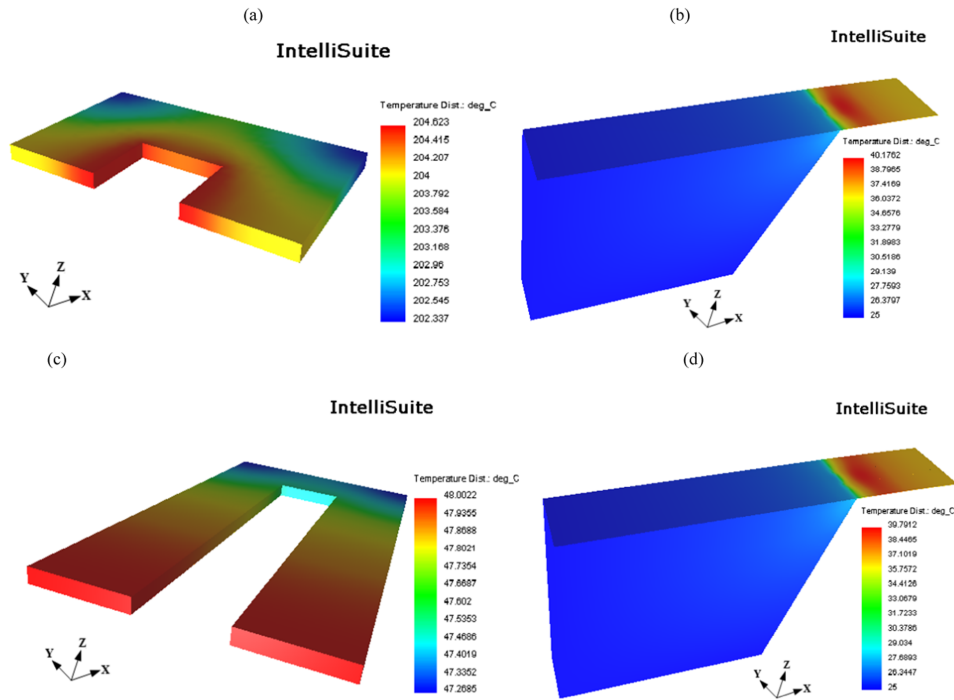


FIG. 4. For $L_p = 60 \mu\text{m}$: temperature profile (a) U-shaped piezoresistor operated in air, and (b) resistor integrated with the cantilever platform. For $L_p = 180 \mu\text{m}$: temperature profile (c) U-shaped piezoresistor operated in air, and (d) resistor integrated with the cantilever platform. In all the above simulations, W_p is fixed at $35 \mu\text{m}$.

numerical simulation, the following observations are made: (i) the analytical eq. (4) models the temperature profile only in the longitudinal direction of the cantilever. However, our simulation results depict that the temperature profile is 3D in nature which is more closer to the practical scenario, and (ii) the magnitude of T_{max} (at $x = L_p$) computed from eq. (4) using Matlab[®] R2013a software and numerical simulation for different L_p (summarized in Table III) shows that eq. (4) not only underestimates T_{max} but also neglects the significance of heat conduction mechanism from the cantilever platform to its base. This negligence results in significant difference in the magnitude of T_{max} between a shorter and lengthier piezoresistor when eq. (4) is used. Therefore, it is concluded that the modeling approach using the numerical simulations not only models the temperature behavior of the sensor better but also gives more insight into the heat transfer mechanism of the sensor.

2. Influence of the piezoresistor width (W_p)

The maximum steady state temperature (T_{max}) of the U-shaped piezoresistor operated in (i) air, and (ii) with the cantilever structural layer and base for different piezoresistor width is shown in Fig 5.

TABLE III. Comparison of analytical model and FEM results of the rectangular cantilever without isolation and immobilization layers for different piezoresistor length.

Piezoresistor dimensions (L_p, W_p) (μm)	Maximum temperature on the rectangular cantilever without isolation and immobilization layers T_{max} ($^{\circ}\text{C}$)		
	Analytical	FEM	% Error (w.r.t FEM)
	Variation in the piezoresistor length, $L_c = 200 \mu\text{m}$, $W_c = 100 \mu\text{m}$, $V_b = 5 \text{ V}$		
(60, 35)	27.1283	40.1762	-32.47%
(90, 35)	28.4208	39.8397	-28.66%
(120, 35)	29.7304	39.7969	-25.29%
(150, 35)	31.0479	39.7932	-21.97%
(180, 35)	32.3697	39.7912	-18.65%

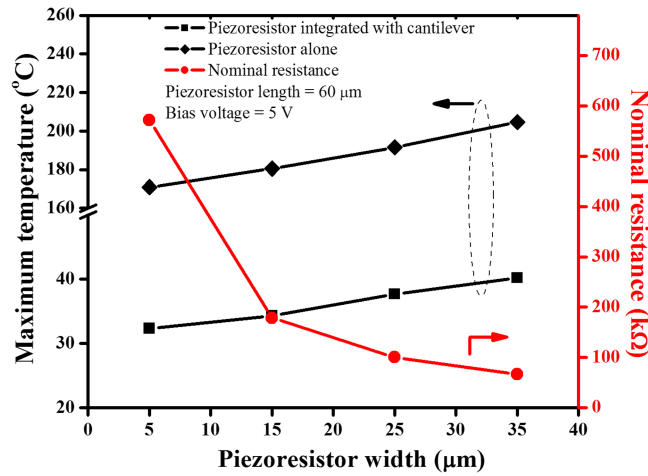


FIG. 5. Maximum cantilever temperature and nominal resistance as a function of the piezoresistor width.

The temperature profiles on the resistor and the cantilever platform for two different piezoresistor widths are shown in Fig 6.

- (i) When the piezoresistor is operated in air, T_{max} increases with increasing W_p . For instance, when W_p increases from 5 μm to 35 μm, R reduces by 8.52 times, and T_{max} increases by 1.19 times. This is due to the fact that as W_p increases, nominal resistance decreases which results in an increase in the magnitude of current flow in the piezoresistor resulting in higher T_{max} .
- (ii) When the piezoresistor is integrated into the cantilever, there is a significant change in the magnitude of T_{max} . First, T_{max} on the cantilever decreases. For instance, at $W_p = 5 \mu\text{m}$, when the piezoresistor is integrated with the cantilever, T_{max} decreases to 32.33°C, which is 81.07%

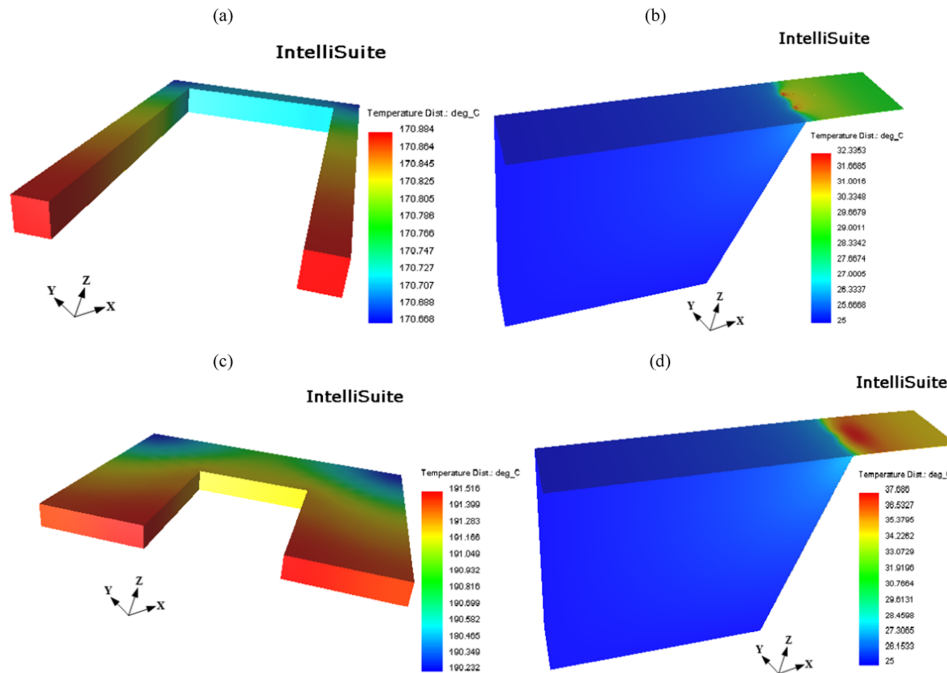


FIG. 6. For $W_p = 5 \mu\text{m}$: temperature profile (a) U-shaped piezoresistor operated in air, and (b) resistor integrated with the cantilever platform. For $W_p = 25 \mu\text{m}$: temperature profile (c) U-shaped piezoresistor operated in air, and (d) resistor integrated with the cantilever platform. In all the above simulations, L_p is fixed at 60 μm.

less than the T_{\max} when the piezoresistor is operated in air. This is due to the higher rate of heat diffusion by conduction. Second, unlike L_P , W_P has significant effect on the magnitude of T_{\max} generated. For example, when the W_P is increased from 5 μm to 35 μm , T_{\max} increases by 24.24%.

- (iii) Fig.6 shows that when the piezoresistor is heated in air, T_{\max} varies within 2% of the average temperature on the piezoresistor surface. However, when the piezoresistor is integrated with the cantilever, compared to L_P , the variation in W_P has significant effect on the temperature profile in terms of temperature non-uniformity. For instance, when $W_P = 5 \mu\text{m}$, T_{\max} is present only at the piezoresistor legs resulting in two hot spots on the cantilever platform. However, for the same W_S , when W_P is increased from 5 μm to 25 μm , the temperature profile is more uniformly distributed, especially towards the width of the cantilever. Thus, the coverage of the piezoresistor on the cantilever platform with increasing W_P plays a significant role in determining the spatial temperature profile.

The following observations are made when we compare the thermal behavior of the cantilever with U-shaped piezoresistor (without isolation and immobilization layers) predicted by the analytical eq. (4) and numerical simulation: (i) our simulation results show that compared to L_P , the variation in W_P has more impact on the temperature profile of the sensor. However, it is evident that eq. (4) overlooks the variation in temperature profile in the transverse direction of the cantilever platform, and (ii) the computation results of T_{\max} (at $x = L_P$) from eq. (4) using Matlab[®] R2013a software and numerical simulation for different W_P (summarized in Table IV) shows that eq. (4) underestimates the magnitude of T_{\max} . Due to this negligence of thermal behaviour in transverse direction, the prediction of T_{\max} by eq. (4) as a function of W_P differs significantly from the simulation results.

It can be concluded that when the U-shaped piezoresistor is embedded with the cantilever, the dominant mode of heat transfer mechanism is conduction. In addition, it is found that compared to L_P , W_P has significant impact on the magnitude of temperature and its profile on the cantilever platform.

B. Influence of the isolation and immobilization layers

Typically, the influence of the isolation and immobilization layers on the device performance has been ignored by researchers for reducing computational complexity. However, these two layers should be considered in the design of surface stress based cantilevers, since it contributes to (i) difference in TCE induced deflection (ΔZ_{TCE}), (ii) shift in neutral axis, (iii) change in thermal boundary conditions, and (iv) variation in resonant frequency.

In the present work, we have carried out simulation analysis by incorporating both the layers in the cantilever to analyze device performance.

1. Device with only the isolation layer

The temperature and displacement profile of the device with the isolation layer alone is shown in Fig 7. Apart from TCE, thermal conductivity (λ) and heat capacity (s) of the constituent layers of the cantilever plays a vital role in determining the device performance. The parameter s of

TABLE IV. Comparison of analytical model and FEM results of the rectangular cantilever without isolation and immobilization layers for different piezoresistor width.

Piezoresistor dimensions	Maximum temperature on the rectangular cantilever without isolation and immobilization layers T_{\max} ($^{\circ}\text{C}$)		
	Analytical	FEM	% Error (w.r.t FEM)
(L_P, W_P) (μm)	Variation in the piezoresistor width, $L_C = 200 \mu\text{m}$, $W_C = 100 \mu\text{m}$, $V_b = 5 \text{ V}$		
(60, 5)	25.3040	32.3352	-21.74%
(60, 15)	25.9120	34.2932	-24.43%
(60, 25)	26.5201	37.6860	-29.62%
(60, 35)	27.1283	40.1762	-32.47%

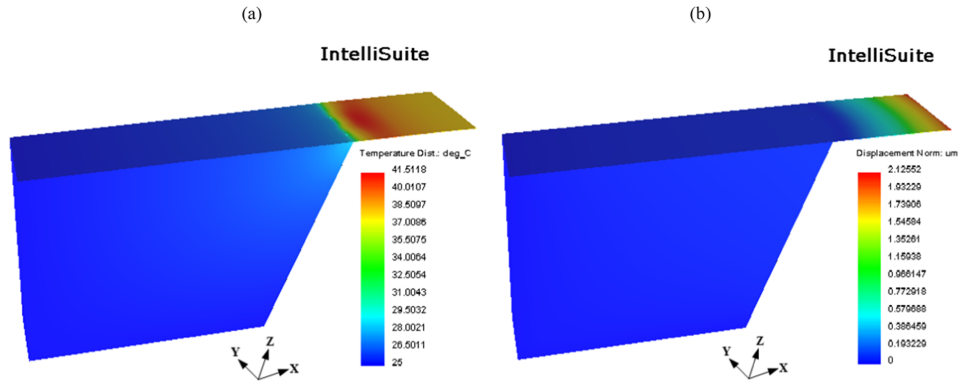


FIG. 7. Simulated (a) temperature and (b) displacement profiles of the cantilever platform with a U-shaped piezoresistor with the addition of the isolation layer.

a material signifies its heat retention capability, whereas λ implies its heat dissipation capability through conduction. Fig 7 shows that when the isolation layer is added, T_{\max} increases. This is due to the combined effect of higher s and lower λ of SiO_2 . Higher s of SiO_2 results in higher T_{\max} , whereas the lower λ adds to the heating of the piezoresistor. Even though, there is an increase in T_{\max} , ΔZ_{TCE} is found to reduce. This is due to the fact that, when only the structural layer (SiO_2) and piezoresistive layer (Si) are present, the cantilever deflects in the downward direction due to higher TCE difference between the top Si layer and the bottom SiO_2 layer. However, the addition of SiO_2 isolation layer, reduces the TCE difference of the composite structure and hence results in reduced ΔZ_{TCE} .

2. Device with the isolation and immobilization layers

The temperature and displacement profile of the device with both the isolation and immobilization layers are shown in Fig 8. When the immobilization layer is added on top of the isolation layer T_{\max} reduces. This is due to the high magnitude of λ of Au immobilization layer which results in higher rate of heat conduction. In addition, the due to higher magnitude of s and lower magnitude of λ of the SiO_2 isolation layer beneath the immobilization layer, which results in reduced heat conduction to the Au immobilization layer. Moreover, it can be seen that, there is an increment in ΔZ_{TCE} . This is due to the high value of TCE of Au, which introduces higher magnitude of mismatch between the materials of the cantilever stack. Since, TCE of Au is greater than SiO_2 and Si, the net cantilever deflection is in the downward direction.

In a composite cantilever, the net deflection is caused by the combination of temperature and net TCE difference of the constituent layers. Details of various combinations of constituent layers along

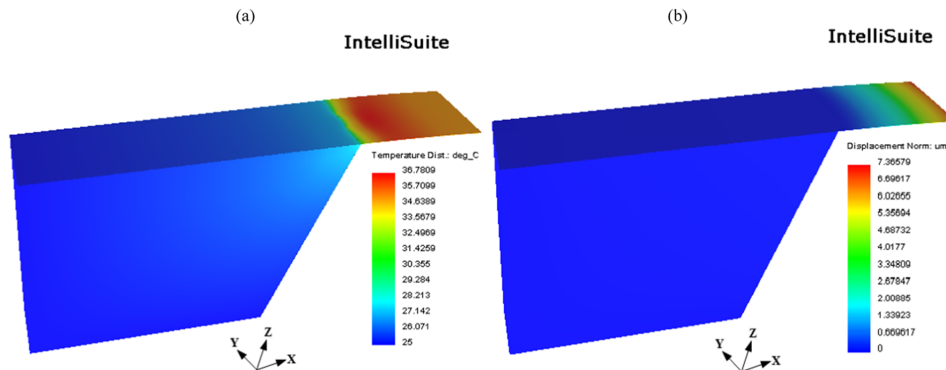


FIG. 8. Simulated (a) temperature and (b) displacement profiles of the cantilever platform with a U-shaped piezoresistor with the addition of both the isolation and immobilization layers.

TABLE V. Magnitude of maximum steady state temperature (T_{\max}) and TCE induced cantilever deflection (ΔZ_{TCE}).^a

Case	Structure details	T_{\max} ($^{\circ}\text{C}$)	$\Delta\alpha$ ($1\text{E-}7/^{\circ}\text{C}$)	ΔZ_{TCE} (μm)
I	Device (structural layer + piezoresistor)	40.17	-23.0	3.37
II	Device + isolation layer	41.51	-17.0	2.12
III	Device + isolation + immobilization layer	36.78	-125.0	7.36

^aPiezoresistor dimensions (in micrometers): (L_p , W_p) = (60, 35).

with their corresponding magnitudes of T_{\max} , net TCE due to bilayer combination ($\Delta\alpha$) and ΔZ_{TCE} are summarized for different scenarios in Table V. The parameter $\Delta\alpha$ is computed as the difference in TCE of the bottom (α_b) and top (α_t) layers given as $\Delta\alpha = \alpha_b - \alpha_t$. From Table V it is observed that when only structural and piezoresistor layers are present (case-I), the magnitude of T_{\max} and ΔZ_{TCE} are $40.17\text{ }^{\circ}\text{C}$ and $3.37\text{ }\mu\text{m}$ respectively with $\Delta\alpha_I = \alpha_{\text{SiO}_2} - \alpha_{\text{Si}} = -23\text{ E-}7/^{\circ}\text{C}$. The $-ve$ sign indicates that the net cantilever deflection is in the downward direction. When the isolation layer is added (case-II), the magnitude of T_{\max} increases, whereas the net ΔZ_{TCE} is found to decrease. This is due to the fact that with the addition of the isolation layer, the parameter $\Delta\alpha_{II} = |\alpha_I| - \alpha_{\text{SiO}_2} = -17\text{ E-}7/^{\circ}\text{C}$ reduces which results in a net reduction in ΔZ_{TCE} . On the other hand, when the immobilization layer is added (case-III), even though T_{\max} reduces, the net ΔZ_{TCE} is found to increase. This is attributed to the increase in the parameter $\Delta\alpha_{III} = |\alpha_{II}| - \alpha_{\text{Au}} = -125\text{ E-}7/^{\circ}\text{C}$ which results in an increase in the magnitude of ΔZ_{TCE} . Furthermore, it is observed that the magnitude of ΔZ_{TCE} varies non-linearly with respect to $\Delta\alpha$. This is due to the increase in the flexural rigidity of the cantilever platform with the addition of the isolation and immobilization layers.

C. Effect of cantilever dimensions on the thermo-mechanical characteristics

In the preceding sections, the sensor response was investigated for fixed cantilever dimensions. In this section, thermal response of the sensor is analyzed as a function of the lateral dimensions of the cantilever platform.

1. Effect of the cantilever length (L_C)

The effect of L_C on the magnitude of T_{\max} and ΔZ_{TCE} are plotted in Fig 9 for different W_p . In all the simulations, L_p is kept constant. For a fixed W_p as L_C is increased, there is a negligible reduction in T_{\max} . Even though, the piezoresistor dimensions are constant, still this reduction in T_{\max} is due to the increase in the surface area of the cantilever on increasing L_C . Increased surface area of the cantilever results in an increase in the convection heat transfer to the ambient. Moreover, as understood

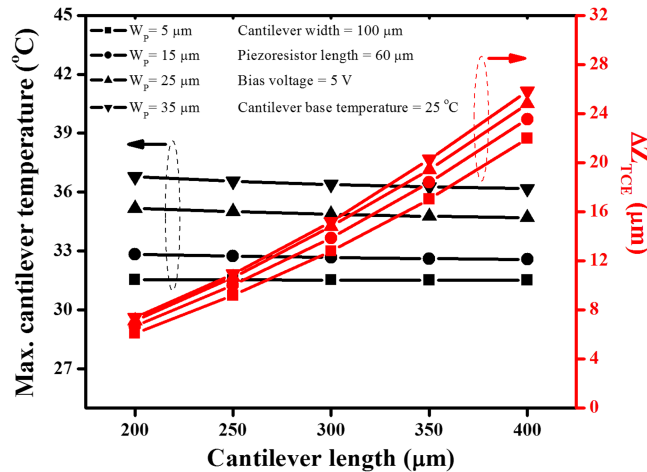


FIG. 9. Variation in the magnitude of maximum steady state cantilever temperature and TCE induced cantilever deflection versus the cantilever length for different piezoresistor width.

from the previous analysis in section VI (A), wider piezoresistors result in higher magnitude of T_{\max} for all L_C . For instance, at $L_C = 400 \mu\text{m}$, when W_P is varied from $5 \mu\text{m}$ to $35 \mu\text{m}$, T_{\max} increases by 14.79%.

Furthermore, for a fixed L_C , when W_P is increased, ΔZ_{TCE} increases due to an increase in T_{\max} . For instance, for $L_C = 400 \mu\text{m}$, when W_P is increased from $5 \mu\text{m}$ to $35 \mu\text{m}$, ΔZ_{TCE} increases by 17.54%. Even though, T_{\max} is almost constant with varying L_C , still there is a significant increase in ΔZ_{TCE} when L_C is increased. This is due to (i) the dependence of ΔZ_{TCE} on the non-uniformity of temperature profile rather than T_{\max} alone, and (ii) reduction in the flexural rigidity of the cantilever with increasing L_C .²⁹ For instance, at $W_P = 35 \mu\text{m}$, when L_C is increased from $200 \mu\text{m}$ to $400 \mu\text{m}$, ΔZ_{TCE} increases by 3.5 times.

2. Effect of the cantilever width (W_C)

The effect of W_C on T_{\max} and ΔZ_{TCE} are plotted in Fig 10 for different L_P . In this analysis, L_C and W_P are fixed at $200 \mu\text{m}$ and $35 \mu\text{m}$ respectively. In all the simulations, the piezoresistor is symmetrically positioned at the center of W_C near the base with $W_S = 30 \mu\text{m}$. It can be noticed that for a fixed L_P , as W_C is increased, there is a reduction in T_{\max} . This is due to (i) an increase in the surface area of the cantilever which results in higher heat transfer through convection, and (ii) an increase in the direct contact area to the cantilever base resulting in higher heat diffusion through conduction. For instance, for a fixed $L_P = 60 \mu\text{m}$, when W_C is varied from $100 \mu\text{m}$ to $200 \mu\text{m}$, T_{\max} reduces by 9.06%. Moreover, it is observed that for a fixed W_C , cantilevers with lower values of L_P exhibits higher T_{\max} . It is evident from Fig 10 that for a fixed L_P , when W_C is increased, there is negligible change in ΔZ_{TCE} . Similar to L_C variation, here also the non-uniformity in temperature profile is increased with increasing W_C . However, there is only a marginal change in ΔZ_{TCE} due to increased flexural rigidity of the cantilever.

From the investigations carried out in section VI(C), it is clear that for composite piezoresistive cantilever biosensors (i) shorter and wider cantilever geometries are better in terms of reduced T_{\max} and ΔZ_{TCE} , and (ii) W_P has higher impact on ΔZ_{TCE} than L_P . Considering the fact that shorter and wider piezoresistors are ideal for surface stress based cantilever biosensors, for further investigation, we have taken a square cantilever platform ($L_C = W_C = 200 \mu\text{m}$) with an integrated U-shaped piezoresistor with L_P and W_S of $60 \mu\text{m}$ and $30 \mu\text{m}$ respectively. Since, W_P plays a critical role in determining the thermal behavior of the sensor, in the subsequent sections we investigate the impact of W_P on the sensitivity factor (v).

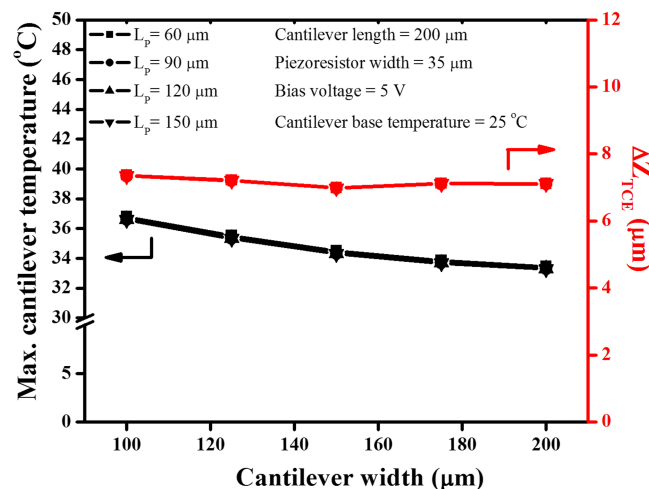


FIG. 10. Variation in the magnitude of maximum steady state cantilever temperature and the TCE induced cantilever deflection versus the cantilever width for different piezoresistor length.

D. Effect of piezoresistor width on sensitivity ratio

In this section, we analyze the influence of W_P on the sensitivity factor (ν) such that ν can be maximized. The factor ν is obtained by computing the ratio of target-receptor interactions induced surface stress to self-heating induced changes in $\Delta R/R$.³⁶ The factors TCP, TCR and TCE contribute to the thermal drift of sensor output. Typically, a piezoresistive cantilever biosensor is connected to one arm of a Wheatstone bridge (WSB) with another reference cantilever operated in differential mode. The other two passive resistors which complete the WSB are realized on the same die.²⁵ Since, all the four resistors are thermally coupled and are in thermal equilibrium with each other, variations in the output, especially due to variations in intrinsic parameters like TCR can be effectively nullified.⁴⁵ Moreover, through our computations it was found that the contribution of TCR to $\Delta R/R$ was less than 1% compared to TCP and TCE induced inaccuracies. Therefore, in this study, we have focused on TCP and TCE induced inaccuracies.

Maximum cantilever tip deflection due to applied surface stress (ΔZ_{OS}) and difference in TCE (ΔZ_{TCE}) as a function of W_P is shown in Fig 11. The plot also contains the specifics of maximum cantilever temperature as a function of W_P . The following observations are made from the simulation results: (i) for an applied surface stress, ΔZ_{OS} remains constant (1.73 μm) irrespective of the variation in W_P , (ii) with an increase in W_P , the parameter ΔZ_{TCE} increases. This is due to the fact that as W_P increases, nominal resistance decreases and the magnitude of current increases which results in higher heat generation, and thereby higher T_{max} . The combined effect of the aforementioned factors with the difference in TCE of constituent materials results in larger ΔZ_{TCE} . For instance, when W_P is increased from 5 μm to 35 μm , the magnitude of T_{max} and ΔZ_{TCE} increases by 7.13% and 14.51% respectively.

The magnitude of $\Delta R/R$ induced due to applied surface stress, and thermal drift components TCP and TCE as a function of W_P is shown in Fig 12. The plot also shows the variation of sensitivity ratio as a function of W_P . It is observed that the magnitude of $\Delta R/R$ increases initially and then falls after $W_P = 15 \mu\text{m}$. This is due to the fact that the factor $\Delta R/R$ is a function of the difference in the longitudinal (σ_{xx}) and transverse (σ_{yy}) stress tensors represented as $\sigma_{xx} - \sigma_{yy}$ as given by eq. (7).^{15,46} From the inset figures of piezoresistor in Fig 12, it is seen that as W_P increases, the transverse piezoresistor section which is parallel to cantilever base increases. Since, for p-type SCS piezoresistors the longitudinal and transverse piezoresistive coefficients have equal but opposite magnitude, the increase in piezoresistor transverse section results in the reduction of $\Delta R/R$. In the present study, the contribution of transverse section becomes significant after $W_P = 15 \mu\text{m}$ which results in a decrease in $\Delta R/R$ at higher W_P .

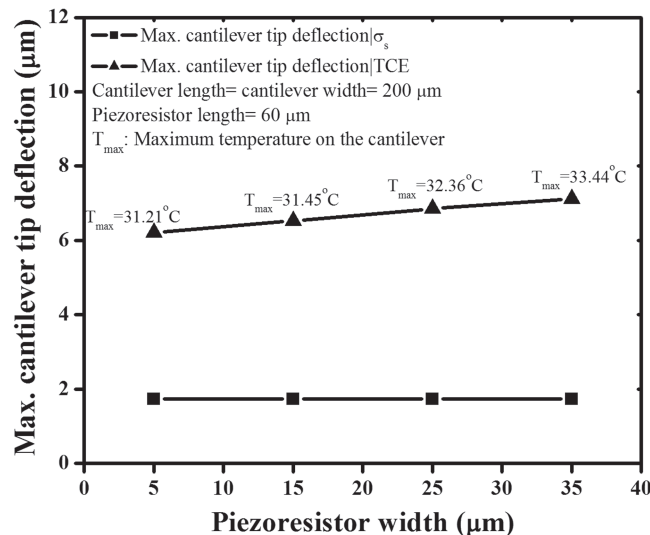


FIG. 11. Variation in the maximum cantilever tip deflection due to surface stress and TCE, and nominal resistance as a function of piezoresistor width.

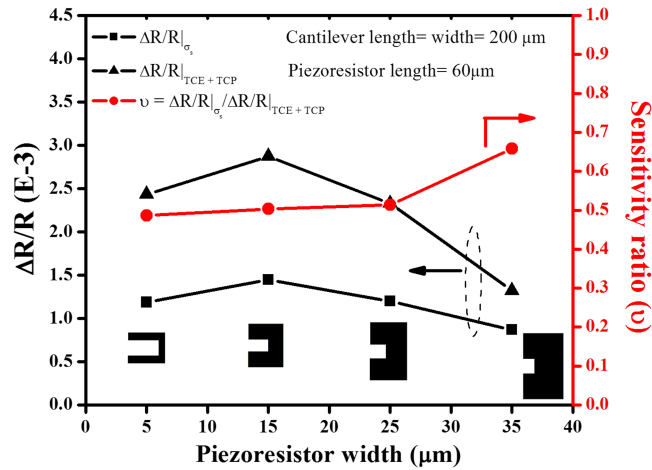


FIG. 12. Variation in the $\Delta R/R$ and sensitivity ratio as a function of piezoresistor width.

Furthermore, it is observed that for fixed L_P as W_P increases, ν improves. This is due to the fact that, at higher values of W_P , the ratio $\Delta R/R|_{\sigma_s}/\Delta R/R|_{TCE+TCP}$ improves. This is mainly due to higher rate of reduction in $\Delta R/R|_{TCE+TCP}$ at larger values of W_P . For instance, when W_P is increased from 25 μm to 35 μm , the magnitude of $\Delta R/R|_{\sigma_s}$ reduces by 27.40%, whereas $\Delta R/R|_{TCE+TCP}$ falls by 43.37%. Therefore, it can be concluded that in order to improve ν of piezoresistive cantilever sensors, wider piezoresistors should be chosen.

E. Operation of the sensor in liquid medium

Further simulations were performed to extend the modeling approach by operating the sensor in liquid environment. For investigation, we have taken a square cantilever platform ($L_C = W_C = 200 \mu\text{m}$) with an integrated U-shaped piezoresistor with L_P , W_S and W_P of 60 μm , 30 μm and 35 μm respectively. Water was chosen as the liquid medium. Typically, the heat convection coefficient of water is 25 times higher than that of air.⁴⁷ Convection heat coefficient of water $h_{\text{water}} = 5000 \text{ W/m}^2 \text{ }^\circ\text{C}$ was imparted to the sensor model. Simulations were carried out and the following observations were made: compared to air when sensor is operated in water (i) the magnitude of T_{max} reduces from 33.44 $^\circ\text{C}$ to 31.12 $^\circ\text{C}$, (ii) magnitude of ΔZ_{TCE} reduces from 7.11 μm to 6.29 μm (iii) magnitude of $\Delta R/R|_{TCE+TCP}$ reduces from 1.31 E-3 to 1.26 E-3, and (iv) sensitivity factor (ν) improves from 0.65 to 0.68. The premise is due to the high convection heat transfer of water compared to air, which results in higher rate of heat dissipation and thereby reduced T_{max} , ΔZ_{TCE} , $\Delta R/R|_{TCE+TCP}$ and higher sensitivity factor (ν). It may be noted that although the sensitivity ratio improves when the sensor is operated in water, the higher viscous damping in liquid medium will reduce the Q-factor and thereby the σ_{min} of the sensor.

In the present work, the maximum sensitivity ratio was obtained as 0.65 (in air) and 0.68 (in water) at a dc-voltage supply of 5 V. The sensitivity ratio of the sensor can be further improved by reducing the supply voltage to 1 V, since at lower supply voltages the contribution of $\Delta R/R|_{TCE+TCP}$ is expected to reduce. Furthermore, lower supply voltage will also improve the minimum detectable surface stress (σ_{min}) and signal to noise ratio (SNR) of the sensor by reducing the intrinsic electrical noises, especially the Hooge's noise due to lower magnitude of joule heating induced temperature on the cantilever platform. Further improvement in σ_{min} and SNR can be achieved by choosing surface doping concentration of the piezoresistor ranging from $1 \text{ E}18 \text{ cm}^{-3}$ to $1 \text{ E}19 \text{ cm}^{-3}$ which will further reduce the Hooge's noise and for the same piezoresistor geometry will reduce the nominal resistance and thereby Johnson's noise. Although, silicon dioxide based piezoresistive cantilevers have been reported to achieve resolution of ng/ml @ 3 V supply voltage,⁴⁸ improvement in the sensor resolution can be achieved by careful design of sensor geometry and reducing the supply voltage. Even though, in the present study we have considered a piezoresistor with a junction depth of 100 nm which can be realized with ion-implantation process,^{24,49-52} the results and conclusions obtained are also valid for

piezoresistors with higher junction depths or piezoresistors realized with two-step thermal diffusion process.

Based on the investigation carried out, we devise a set of design guidelines to effectively model and design composite piezoresistive cantilever sensors:

- (i) To effectively model the sensor closer to practical scenario the following aspects should be considered during the modeling stages:
 - (a) Sensor should be modeled with its mechanical base in such a way that the sensor mechanical base acts as a perfect heat sink to ensure conduction mode of heat dissipation.
 - (b) Both isolation and immobilization layers should be taken into account in the modeling and design stages due to their prominent role in TCE induced cantilever deflection.
 - (c) The external environment in which the sensor is operated should be considered in the modeling stages since it not only determines the convection mode of heat dissipation but also governs the fluid damping effect and thereby the minimum detectable surface stress.
- (ii) Piezoresistor length (L_P) has negligible impact on the maximum temperature on the cantilever platform (T_{\max}) and thereby maximum cantilever tip deflection due to TCE (ΔZ_{TCE}), but to ensure higher magnitude of electrical sensitivity: $L_P/L_C \leq 0.33$.
- (iii) To ensure high value of sensitivity ratio (ν), piezoresistor width (W_P) should be large taking into account the rise in T_{\max} due to susceptibility of target-receptor interactions to temperature changes.

To summarize, we believe that the multi-physics modeling approach and the results reported in the present work will enable NEMS design engineers to model and design piezoresistive cantilever biosensor with better performance. Even though, we have considered the specific case of piezoresistive cantilever biosensor, the results obtained in this work and the modeling approach devised is extendable to other piezoresistive based sensors. Future work includes design and optimization of piezoresistive silicon dioxide sensors considering thermal drift and its dependence on the sensor geometry.

VII. CONCLUSION

This paper elucidates the impact of self-heating on the performance of piezoresistive cantilever biosensors through 3D multi-physics modeling. Simulation results show that in piezoresistive cantilever sensors, conduction mode of heat transfer plays a critical role in governing the magnitude of temperature and its profile. Similarly, it is depicted that the isolation and immobilization layers have profound impact on the thermo-mechanical response of the sensor. Especially, the gold immobilization layer is found to be the major contributor to the TCE induced deflections. A systematic investigation is carried out to understand the influence of the relative dimensions of the piezoresistor and the cantilever on the sensor performance using a FEM based numerical simulation tool. Results show that shorter and wider cantilevers are more suitable to minimize the self-heating induced inaccuracies, especially the TCE induced deflections. In addition, it is found that the piezoresistor width is important in determining the thermal behaviour. It has been demonstrated that the wider piezoresistor improves the electrical sensitivity to thermal sensitivity ratio, and thereby the sensor performance.

¹ Z. W. Liu, Z. Y. Tong, B. Liu, L. Q. Hao, X. H. Mu, J. P. Zhang, and C. Gao, *AIP Advances* **5**, 041324 (2015).

² T. Akiyama, S. Gautsch, N. F. de Rooij, U. Staufer, Ph. Niedermann, L. Howald, D. Muller, A. Tonin, H. R. Hidber, W. T. Pike, and M. H. Hecht, *Sensors and Actuators A* **91**, 321 (2001).

³ J. L. Arlett, E. B. Myers, and M. L. Roukes, *Nature Nanotechnology* **6**, 203 (2011).

⁴ H. P. Lang, M. K. Baller, R. Berger, C. Gerber, J. K. Gimzewski, F. M. Battiston, P. Fornaro, J. P. Ramseyer, E. Meyer, and H. J. Guntherodt, *Analytica Chimica Acta* **393**, 59 (1999).

⁵ S. Xu and R. Mutharasan, *Environ. Sci. Technology* **44**, 1736 (2010).

⁶ S. J. Kim, T. Ono, and M. Esashi, *Applied Physics Letters* **88**, 053116 (2006).

⁷ M. Maute, S. Raible, F. E. Prins, D. P. Kern, H. Ulmer, U. Weimar, and W. Gopel, "Detection of volatile organic compounds (VOCs) with polymer-coated cantilevers detector," *Sensors and Actuator B* **58**, 505–511 (1999).

⁸ S. Kim, D. Yi, A. Passian, and T. Thundat, "Observation of an anomalous mass effect in microcantilever-based biosensing caused by adsorbed DNA," *Applied Physics Letters* **96**, 153703 (2010).

- ⁹ H. S. Wasisto, S. Merzsch, A. Waag, E. Uhde, T. Salthammer, and E. Peiner, "Portable cantilever-based airborne nanoparticle detector," *Sensors and Actuator B* **187**, 118–127 (2013).
- ¹⁰ H. J. Pandya, W. Chen, L. A. Goodell, D. J. Foran, and J. P. Desai, *Lab on a Chip* **14**, 4523 (2014).
- ¹¹ N. Bajwa, C. J. Maldonado, T. Thundat, and A. Passian, *AIP Advances* **4**, 037118 (2014).
- ¹² K. W. Wee, G. Y. Kang, J. Park, J. Y. Kang, D. S. Yoon, J. H. Park, and T. S. Kim, *Biosensors and Bioelectronics* **20**, 1932 (2005).
- ¹³ R. Mukhopadhyay, M. Lorentzen, J. Kjems, and F. Besenbacher, *Langmuir* **21**, 8400 (2005).
- ¹⁴ Z. Q. Tan, N. H. Zhang, W. L. Meng, and H. S. Tang, *J. Phys. D: Appl. Phys.* **49**, 225402 (2016).
- ¹⁵ F. T. Goericke and W. P. King, *IEEE Sensors Journal* **8**, 1404 (2008).
- ¹⁶ A. R. Sankar and S. Das, *Sensors and Actuators A* **189**, 125 (2013).
- ¹⁷ S. M. Yang and T. I. Yin, *Sensors and Actuators A* **120**, 736 (2007).
- ¹⁸ M. Z. Ansari and C. Cho, *J. Phys. D: Appl. Phys.* **44**, 285402 (2011).
- ¹⁹ M. Z. Ansari and C. Cho, *Sensors and Actuators A* **175**, 19–27 (2012).
- ²⁰ A. Johansson, O. Hansen, J. Hales, and A. Boisen, *Journal of Micromechanics and Microengineering* **16**, 2564–2569 (2006).
- ²¹ A. Loui, S. Elhadj, D. J. Sirbully, S. K. McCall, B. R. Hart, and T. V. Ratto, *Journal of Applied Physics* **107**, 054508 (2010).
- ²² J. C. Doll, E. A. Corbin, W. P. King, and B. L. Pruitt, *Applied Physics Letters* **98**, 223103 (2011).
- ²³ S. M. Yang, C. Chang, and T. I. Yin, *Sensors and Actuators B* **129**, 678 (2008).
- ²⁴ Y. Zhou, Z. Wang, C. Wang, W. Ruan, and L. Liu, *Journal of Micromechanics and Microengineering* **19**, 065026 (2009).
- ²⁵ J. Thaysen, A. Boisen, O. Hansen, and S. Bouwstra, *Sensors and Actuators A* **83**, 47 (2000).
- ²⁶ J. C. Love, L. A. Estroff, J. K. Kriebel, R. G. Nuzzo, and G. M. Whitesides, *Chemical Reviews* **105**, 1103 (2005).
- ²⁷ J. Thaysen, A. D. Yalcinkaya, P. Vettiger, and A. Menon, *J. Phys. D: Appl. Phys.* **35**, 2698 (2002).
- ²⁸ R. Mathew and A. R. Sankar, *J. Phys. D: Appl. Phys.* **48**, 205402 (2015).
- ²⁹ Z. Wang, R. Yue, R. Zhang, and L. Liu, *Sensors and Actuators: A* **120**, 325–336 (2005).
- ³⁰ J. Thaysen, Ph.D. dissertation (Mikroelektronik Centre, Technical Univ. Denmark, Lyngby, Denmark, 2001).
- ³¹ S. M. Yang, T. I. Yin, and C. Chang, *Sensors and Actuators B* **123**, 707 (2007).
- ³² P. A. Rasmussen, J. Thaysen, O. Hansen, S. C. Eriksen, and A. Boisen, *Ultramicroscopy* **97**, 371 (2003).
- ³³ M. Joshi, P. S. Gandhi, R. Lal, V. Ramgopal Rao, and S. Mukherji, *J. Microelectromech. Syst.* **20**, 774 (2011).
- ³⁴ G. Villanueva, J. A. Plaza, J. Montserrat, F. Perez-Murano, and J. Bausells, *Microelectronic Engineering* **85**, 1120 (2008).
- ³⁵ N. L. Privorotskaya and W. P. King, *Sensors and Actuators A* **152**, 160 (2009).
- ³⁶ R. Mathew and A. R. Sankar, *Biomedical Physics & Engineering Express* **2**, 055012 (2016).
- ³⁷ Y. Arntz, J. D. Seelig, H. P. Lang, J. Zhang, P. Hunziker, J. P. Ramseyer, E. Meyer, M. Hegner, and C. Gerber, *Nanotechnology* **14**, 86 (2003).
- ³⁸ J. Lee and W. P. King, *Sensors and Actuators A* **136**, 291 (2007).
- ³⁹ A. Loui, F. T. Goericke, T. V. Ratto, J. Lee, B. R. Hart, and W. P. King, *Sensors and Actuator A* **147**, 516 (2008).
- ⁴⁰ M. A. Hopcroft, W. D. Nix, and T. W. Kenny, *J. Microelectromechanical Systems* **19**, 229 (2010).
- ⁴¹ Y. Kanda, *IEEE Trans. Electron. Devices* **29**, 64 (1982).
- ⁴² V. Chivukula, M. Wang, H. F. Ji, A. Khaliq, J. Fang, and K. Varahramyan, *Sensors and Actuator A* **125**, 526 (2006).
- ⁴³ Y. Zhou, Z. Wang, Q. Zhang, W. Ruan, and L. Liu, *IEEE Sensors Journal* **9**, 246 (2009).
- ⁴⁴ P. Norton and J. Brando, *Solid State Electronics* **21**, 969 (1978).
- ⁴⁵ B. W. Chui, L. Aeschmann, T. Akiyama, U. Staufer, and N. F. de Rooij, *Review of Scientific Instruments* **78**, 043706 (2007).
- ⁴⁶ M. J. Madou, *Fundamentals of microfabrication*, 2nd ed. (CRC press), chapter 4, pp.201.
- ⁴⁷ J. C. Doll and B. L. Pruitt, *Piezoresistor design and applications, Microsystems and nanosystems* (Springer), chapter 5, pp.140.
- ⁴⁸ R. Zhao, W. Ma, Y. Wen, J. Yang, and X. Yu, *Sensors and Actuators B: Chemical* **212**, 112 (2015).
- ⁴⁹ G. Zuo, X. Li, P. Li, T. Yang, Y. Wang, Z. Cheng, and S. Feng, *Analytica Chimica Acta* **580**, 123 (2006).
- ⁵⁰ Y. Yang, Y. Chen, P. Xu, and X. Li, *Microelectronic Engineering* **87**, 2317 (2010).
- ⁵¹ Y. Chen, P. Xu, M. Liu, and X. Li, *Microelectronic Engineering* **87**, 2468 (2010).
- ⁵² D. F. Downey U.S. Patent 6,069,062, issued May 30 (2000).